Materials & Design 260 (2025) 115107

Contents lists available at ScienceDirect

Materials & Design

journal homepage: www.elsevier.com/locate/matdes

Process stability and limits of agglomerating 316L powder in laser powder bed fusion of metals

Kai Drechsel*, Volker Schulze, Frederik Zanger

wbk - Institute of Production Science, Kaiserstraße 12, 76131, Karlsruhe, Germany

HIGHLIGHTS

- A stable process window for the processing of a resource efficient, but agglomerating, 316L powder was determined.
- A mechanism defining process limits for the agglomerating powder was identified.
- The critical influence of the oxygen content in the build chamber on the process stability for 316L powder with a large amount of fine particles was demonstrated.

GRAPHICAL ABSTRACT

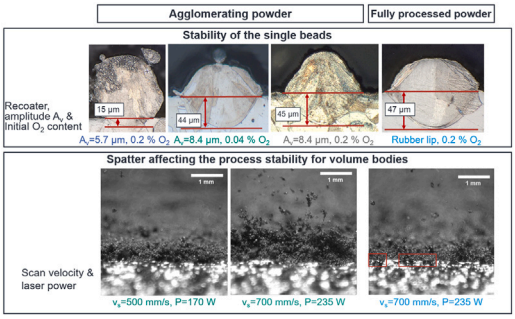

ARTICLE INFO

Keywords:
Ultrasonic recoating
Humping
Resource efficiency
PBF-LB

ABSTRACT

Process stability and maximum productivity are fundamental requirements for laser powder bed fusion of metals (PBF-LB\M). The influence of particle size distribution and process parameters have been investigated in many studies. However, these findings are limited to spreadable powder. For agglomerating powders, due to a large number of fine particles, recoating is not possible with a conventional recoater. To overcome this obstacle, an ultrasonically excited recoating system was developed, in previous work. The processing of such powder is desirable, as the yield of atomization can be increased by about 24 %. To evaluate the process stability and limits, single beads and volume bodies were manufactured. A stable process window, achieving a high relative density, was determined. A critical influence of the O_2 concentration in the build chamber and the vibration amplitude of the ultrasonic recoater was found. The productivity is limited by the process induced powder movement, due to the formation of a powder wall.

1. Introduction

A near net shape manufacturing of complex geometries is enabled by laser powder bed fusion of metals (PBF-LB\M according to ISO 52900, formerly known as laser powder bed fusion (LPBF)). Powder properties, such as particle size distribution (PSD), particle shape, flowability and chemical composition significantly influence process stability and part quality during the recoating and melting process of PBF-LB\M [1–3]. A positive effect on the density of fine powders was found by [1,4,5], while [6] found the opposite effect. However, recoating issues were identified for powders containing too many fine particles. The large number of fine particles causes the powder to agglomerate and the spreadability is no longer ensured. Therefore, previous studies are usually limited to flowable powders [3,5].

* Corresponding author.
Email addresses: Kai.Drechsel@kit.edu (K. Drechsel), Volker.Schulze@kit.edu (V. Schulze), Frederik.Zanger@kit.edu (F. Zanger).

https://doi.org/10.1016/j.matdes.2025.115107
Received 26 February 2025; Received in revised form 23 September 2025; Accepted 7 November 2025
Available online 10 November 2025

An ultrasonically excited recoating system for PBF-LB\M to process non-spreadable powder was developed in a previous study [7]. The system was used to recoat 316 L powder with a large number of fines smaller than 20 µm, which caused agglomeration due to van der Waals forces [8]. However, only the recoating process was investigated on a specially designed test bench. This powder represents a resource efficient powder, since none of the about 24 % fine particles smaller than 20 µm produced in the atomization process were removed. Another way to increase resource efficiency is the recycling of powder [9].

The processability during the melting of such an agglomerating powder is not yet investigated. Other studies, mentioned earlier, reported issues with the recoateability but proceeded to process the powder despite the defects. There is a gap in knowledge, as those results were affected by the recoating defects. Large particles had a negative impact on the melt pool stability of 316 L, causing the width to be less even throughout a weld track [1]. The melt pool stability is crucial for the microstructure and mechanical properties and is influenced by vaporization [10]. Metal vaporization has significant effects on powder denudation, plume, spatter, lack of fusion porosity. For a stable PBF-LB\M process, an adequate laser energy input as well as an efficient gas circulation system are necessary to suppress the negative effect of vaporization and achieve stable formation quality [10].

Vaporization occurs due to the localized laser melting within tens of microseconds [11]. The vaporization is especially strong under keyhole conditions [12]. The force of the vapor plume acts only within 1 mm above the melt pool, but has a strong drag force [13]. This drag force ejects both hot spatter (molten droplets) and cold spatter (powder particles) away from the laser spot [14]. The spattering increases for higher volume energy densities. Processing of 316 L creates more spatter than aluminum, due to the lower vaporization enthalpy [14]. Also, molten 316 L droplets are more likely to be ejected than aluminum, due to the higher viscosity of the molten 316 L and therefore worse incorporation into the melt pool. The surface tension related issues are also known in the area of TIG welding, where an oxidizing flux is added to alter the surface tension and to improve penetration depth of the melt pool [15].

The vapor plume induces a gas flow with a time delay of a few hundred microseconds after the laser heats the area [11]. This gas flow drags particles towards the laser spot [11,14]. It is the main effect that drags powder particles out of the powder layer, creating powder-free zones and accumulations of particles [16]. This has a critical influence on process stability, since it results in uneven layer thickness and unstable melting behavior, causing formation defects [16]. The spatter can lead to defects, due to its large size compared to the powder [17].

The presented research is a direct succession of the results of [7]. In [7] only the recoating process was investigated. This study focuses on the melting behavior of agglomerating powder and the manufacturing of volume bodies, including cold spatter. The novelty lies in the extension to a non-spreadable powder. A combined approach of single beads and volume bodies, is typically used to understand how different process parameters, scanning patterns, and powder feedstock affect powder melting behavior, molten liquid flow, and pore formation [18]. First, the process stability of the agglomerating powder is investigated through single bead experiments. The melt track height, depth and contact width were examined for different recoating process parameters as well as various oxygen contents. Second, volume bodies were manufactured to determine a process window and the processing limits for agglomerating powder. The process parameters for the recoating and melting processes were varied. All results were compared with standard powder.

2. Material and method

2.1. Powder properties

The two powders used are identical to those used in our previous study [7]. Both powders are made from the same batch of raw powder. The first powder is called powder A. This powder is sieved and air classified to remove all particles after the atomization which are too large or too small for the process [7]. This powder represents a standard powder. The second powder is called powder B. For this powder, only the large particles were removed with the same mesh size as for powder A [7]. Powder B is very cohesive and agglomerates, due to the presence of fine particles and therefore relevant van der Waals forces compared to the gravitational force [8]. This powder cannot be recoated with a conventional recoater due to the agglomeration [7]. The chemical composition (Table 1) is taken from [7]. The oxygen content was measured for both powders.

The PSDs and the sphericity value ($SPHT_3$), the span (S_3) and the specific surface area (S_v) of both powders, shown in Table 2, were taken from [7] as well. The presented diameter is x_{area}, which is the diameter of a circle with an equivalent area to that of the particle [23]. The particle diameters at 10 %, 50 %, and 90 % total volume of the powder are represented by d_{10}, d_{50} and d_{90}.

The apparent and tap density were measured according to [24,25] for powders A and B. To determine the powder layer density (PLD), a cavity with a depth of 100 µm and an inner diameter of 35 mm was recoated on a test bench introduced in [7]. The cavity was fixed in place and the recoater was positioned above the rim of the cavity in order to completely fill it with powder but to leave no powder on the rim. The recoater was driven by a linear axis. The recoating velocity ranged from $v_r = 70$ mm/s to $v_r = 250$ mm/s. Powder B was processed with the sonotrode with an amplitude of $A_v = 5.7$ µm and $A_v = 8.4$ µm. Powder A was processed with a rubber lip. The volume of the cavity was 97.820 mm^3 and the tare weight of 65.7148 g was measured with a precision scale (Mettler Toledo XSR204). After the cavity was filled with powder, the weight of the powder was measured and the density was calculated.

2.2. Machine integration of the ultrasonic recoater

Based on the results of [7], a sonotrode with sharp edge with a 60 ° angle was used for the experiments (Fig. 1(a)). The sonotrode vibrates at 35 kHz with an adjustable amplitude in order to temporarily dissolve the agglomerates in powder B. Powder B requires ultrasonic excitation to be recoated. Details about the recoating mechanism can be found in [7]. The best layer quality, by the means of defect rate of the layer, the segregation and PLD, could be achieved with amplitudes between

Table 2
Particle size distribution, span S_3, sphericity $SPHT_3$, and specific surface area S_v of both powders [7].

Powder	d_{10}	d_{50}	d_{90}	S_3	$SPHT_3$	S_v
A	20.25 µm	33.55 µm	57.52 µm	1.111	0.9107	193 1/mm
B	9.96 µm	24.46 µm	49.62 µm	1.622	0.9322	319 1/mm

Table 1
Chemical composition of the powders in mass %. Only the oxygen content was measured for both powders separately [7].

	Fe	C	Cr	Ni	Mo	Mn	Si	N	O
Method	calculated	[19]		[20]			[21]	[22]	
Required	Bal.	≤0.03	16.5 - 18.5	10.0 - 13.0	2.0 - 2.5	≤2.0	≤2.0	≤0.1	–
Powder A	68.6	0.017	16.8	10.6	2.12	1.52	0.32	0.031	0.034
Powder B									0.048

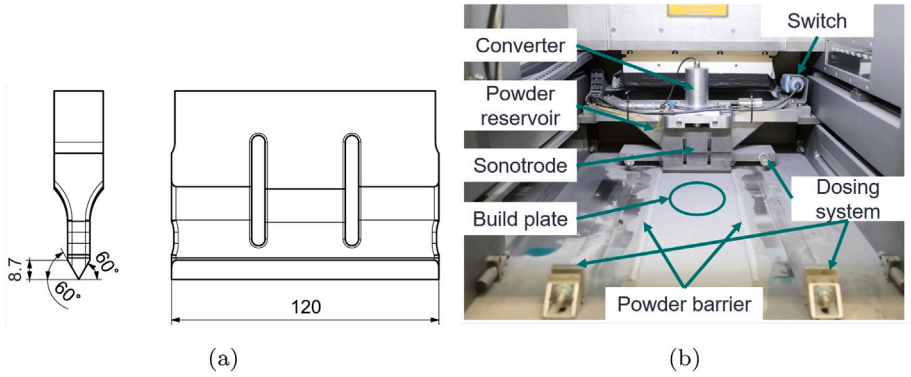

Fig. 1. a) Technical drawing of the sonotrode used for the PBF-LB \M recoating process. b) Integration of the ultrasonic equipment in the SLM280HL.

A_v = 5.7 µm and A_v = 8.4 µm. The sonotrode, made from SPM450V, had a width of 120 mm to cover the entire build plate, which had a diameter of 100 mm.

The experiments were conducted on a SLM280HL 1.0 from Nikon SLM Solutions AG (Lübeck, Germany). The original recoating and powder dosing system did not allow for the integration of the ultrasonic recoating system, so a custom integration was designed (Fig. 1(b)) which was also used in [26]. A carriage frame was fixed on the mounting points of the original recoater. This frame houses a powder tank with a volume of 1.4 l and a mounting block to clamp the converter with two flat ball screws. The powder was dosed using exchangeable metal plates with a rectangular dosing slit of varying sizes. To deposit the powder in front of the recoater, the metal plate is pushed forward by two anchor points (marked as dosing system in Fig. 1(b)) on the forward stroke. During the recoating on the backward stroke, two springs push the dosing slit back under the powder tank to refill it for the next layer. The chosen dosing volume was 595 mm^3, which was sufficient to cover the entire area with powder. Both powders were processed with this setting, only the recoater was exchanged as described.

2.3. Single bead investigations

For the investigation of the process stability, single beads with a length of 20 mm and a distance of 2 mm between each single bead were manufactured. The build plates were made from 316L and ground flat on both sides to ensure a constant layer thickness. The build plate was mounted in the machine and the recoater was placed on top and fixed in position with the two flat ball screws. Afterward, the build plate was lowered by 100 µm, ensuring a reproducible layer thickness. The actual layer thickness during the PBF-LB\M process is thicker than the set nominal layer thickness of s = 50 µm, due to the difference in density between the powder layer and the molten material [27]. Therefore, a layer thickness of s = 100 µm was chosen for all single bead experiments. The varied process parameters are shown in Table 3. A full factorial experimental design was chosen for each powder. The oxygen content was varied between 0.04 % (steady state during the build jobs) and 0.2 % (maximum O_2 content to start the machine). Powder A was only recoated with the rubber lip. This setting represents the standard for the powder and the recoater and was chosen as a benchmark. The processing of powder A with a sonotrode is not the scope of this study. Therefore, a comparison always includes both the powder and recoater.

The weld track shape above the build plate was measured using 3D microscope images from a Keyence VHX-7000 with a 100 x magnification. The height profile was measured on the top of the single beads. The melt pool depth and width were measured in three cross-sections using the Keyence VHX-7000 with a 1000 x magnification. For this analysis, the build plates with the single beads were cut into pieces, ground, polished and etched with V2A-etchant.

2.4. Investigation of volumetric bodies

To investigate the process stability and limits for the manufacturing of volume bodies, cuboids 10×10×10 mm^3 were manufactured. The distance on the build plate was set to 5 mm. The varied process parameters are shown in Table 4. Each parameter was repeated five times. After the manufacturing, the cuboids were cut from the build plate by wire electro-discharge machining. All experiments with the single bead and volume bodies presented in this work were carried out with virgin powder.

The PSD of the deposited powder after a build job was measured. Therefore, additional test specimens were manufactured using the process parameters that resulted in high density and hardness. As the scope of this test was the change in PSD, only the PSD of the batch was measured after the second cycle.

The density of the cubes was measured using the Archimedes Principle according to

$$\rho_s = (\rho_{fl} - \rho_a)\frac{W_a}{W_a - W_{fl}} + \rho_a \quad (1)$$

The density of the solid is ρ_s, the temperature dependent density of the deionized water ρ_{fl} [28], the density of the air ρ_a [29], the weight measured submerged in water W_{fl} and the weight measured in air W_a. A precision scale (Kern ABT 220-5DNM) with an accuracy of 0.1 mg was

Table 3
Varied process parameters for the single bead investigations.

	Powder A	Powder B
Recoater	rubber lip	sonotrode
Amplitude A_v	–	5.7 µm, 7.1 µm and 8.4 µm
Recoating velocity v_r	70 mm/s	
Oxygen content in build chamber	0.04 % and 0.2 %	
Scan speed v_s	700 mm/s	
Laser power P	25 W to 305 W in steps of 10 W	
Layer thickness s	100 µm	

Table 4
Varied process parameters for the volume body investigation.

	Powder A	Powder B
Recoater	rubber lip	sonotrode
Amplitude A_v	–	7.1 µm and 8.4 µm
Recoating velocity v_r	70 mm/s and 105 mm/s	
Oxygen content in build chamber	0.04 % and 0.2 %	
Scan speed v_s	500 mm/s, 600 mm/s and 700 mm/s	
Laser power P	130 W to 230 W in steps of 20 W 180 W to 280 W in steps of 25 W	
Hatch distance h	0.12 mm and 0.14 mm	
Layer thickness s	50 µm	

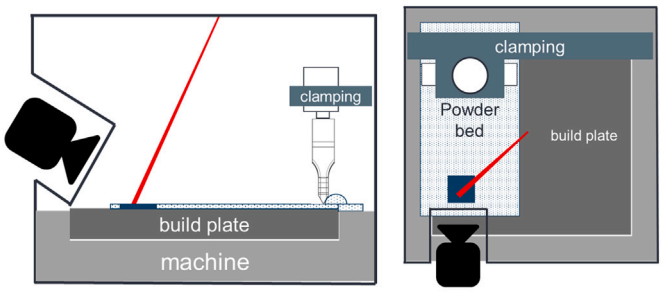

Fig. 2. Integration of the high-speed camera into the SLM280HL 1.0: a) view from the side to show the camera angle and b) view from the top to show the position in the build chamber.

Table 5
Process parameters for the high-speed camera videos.

Process parameter	Condition 1	Condition 2
Laser power P	170 W	235 W
Scan velocity v_s	500 mm/s	700 mm/s
Hatch distance h	0.12 mm	
Layer thickness s	50 µm	
Recoating velocity v_r	70 mm/s	

used. To avoid air bubbles attached to the surface, the cubes were wetted in an ultrasonic bath.

The cubes with the highest density were ground, polished. The defects were investigated using a Keyence VHX-7000 with a 500x magnification.

2.5. High-speed camera investigation

To investigate the powder movement during the manufacturing of a volume body, the melting process was observed with a high-speed camera (Photron FASTCAM NOVA S16). A lens with a12x optical zoom (Navitar 12X Zoom), a 0.75x magnification and a filter for 1070 nm wavelength was used. The working distance of 165 mm was limited by the machine geometry, the capture angle was 30°, and the focus depth was 0.19 mm. A custom-built access for the camera through a tube mounted on the openings of the machine door and a carriage frame to position the sonotrode in front of the camera was designed (Fig. 2). The design is based on the concept of [30], but modified and rebuilt for the new recoating system. For this experiment, the original 280×280 mm^2 build plate was used. The powder deposition was done manually through a glove access on the right side of the door. The powder surface was not measured before scanning. Based on a visual inspection, the powder layer appeared even.

Ten layers were built to ensure a steady state of the layer thickness before the video was captured. An area of 2 × 2 mm^2 was melted. Two different process conditions were tested for both powders (Table 5). Powder B was recoated with an amplitude of A_v = 8.4 µm, powder A was recoated without ultrasonic excitation.

3. Results

3.1. Melt pool shape and stability with single beads

3.1.1. Melt pool height

The height profiles of the single beads manufactured with $P = 205$ W show a significant influence of the amplitude of the sonotrode and the oxygen content in the build chamber (Fig. 3).

For A_v = 5.7 µm and 0.2 % O_2 severe balling (instability at low laser power) or humping (instability at high laser power) occurs with a maximum height of 167 µm. For a reduced oxygen content, the single bead height decreases to a maximum of 119 µm, but balling or humping still occurs. Both single beads have a maximum thickness larger than the powder layer, and the droplets are distorted. This distortion happens due to the unstable melt pool. For $A_v = 8.4$ µm the melt pool stabilizes with increased laser power for both oxygen levels. The maximum heights of the single beads are lower than the thickness of the powder layer, like this is the case for the single beads with powder A. The recoating process itself is not influenced by the oxygen content.

The average height of the single bead over the laser power is shown in Fig. 4. The average height of the single beads manufactured with $A_v = 5.7$ µm and 0.2 % O_2 is slightly above the layer thickness starting from $P = 125$ W. The large scatter indicates the occurrence of balling or humping for all tested laser powers. No process window with a stable melt pool could be found. The minimum laser power required for the melt pool to fuse with the built plate, indicated by a height of zero in Fig. 4, is $P = 95$ W compared to the $P = 35$ W for $A_v = 8.4$ µm and 0.2 % O_2 and $P = 65$ W for powder A with 0.2 % O_2. For $A_v = 5.7$ µm and 0.04 % O_2 the average height is reduced for all scan velocities. For the higher amplitudes, the melt pool stabilizes with an increase in laser power.

3.1.2. Melt pool depth

To further analyze the melt pool stability and the cause of the balling and humping for low amplitudes, the melt pool depth was measured (Fig. 5). For $A_v = 5.7$ µm the melt pool depth is on average about 30 µm lower at $P = 155$ W and $P = 205$ W as for $A_v = 8.4$ µm and powder A recoated with the rubber lip.

With an amplitude of $A_v = 8.4$ µm the melt pool depth is similar to the process with powder A. The change from conduction mode to keyhole mode occurs between $P = 180$ and 205 W for powder B with $A_v = 5.7$ µm, while powder A and powder B with $A_v = 8.4$ µm do not show such a transition in the investigated range. This can be observed by the steep increase of the melt pool depth between $P = 155$ and 180 W in Fig. 6.

3.2. Process limits for volume bodies

3.2.1. Relative density and microstructure

After the analysis of the stability for single beads, the process limits for the manufacturing of volume bodies were investigated. For all build jobs, unless specified differently, an initial oxygen content of 0.04 % was used. Since 316L is a well-understood material in literature [1,31], a comprehensive study of the influence of the process parameters is not the focus of this work. Therefore, the presented results are reduced to the most relevant with the on average highest densities. The error bars represent the standard deviation.

For powder A, the standard parameter set on the SLM280HL 1.0 is a scan velocity of $v_s = 700$ mm/s, a laser power of P = 235 W, a hatch distance of h = 0.12 mm, a layer thickness of $s = 50$ µm and a recoating velocity of $v_r = 70$ mm/s. This parameter set resulted in the highest average density and low scatter for powder A, recoated with the rubber lip (Fig. 7). Powder A has a wide process window between P = 205 W and $P = 280$ W. For a scan velocity of $v_s = 600$ mm/s similar densities can be achieved. The process window is shifted to lower laser powers, as expected [31].

For powder B, recoated with the sonotrode, a large powder barrier formed on each side of the sonotrode (Fig. 1(b)), due to an increased movement of the powder to the side. To ensure a steady powder layer, the recoating of the initial layer was repeated 40 times to form the powder wall.

A scan velocity of v_s = 600 mm/s, an amplitude of A_v = 8.4 µm and recoating velocity of v_r = 105 mm/s results in the highest density. The density achieved with powder B is even higher than for powder A. In the first build job, the laser power was varied between $P = 130$ W and $P = 210$ W. In a second build job, higher laser powers were tested. However, only $P = 220$ W could be manufactured. For

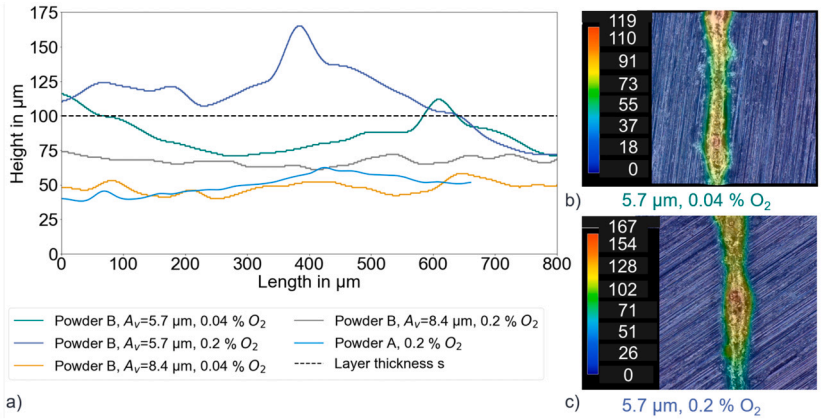

Fig. 3. a) Height profiles of the single beads for different powders, amplitudes and oxygen contents at $P = 205$ W. Image of the single bead for $A_v = 5.7$ µm, $P = 205$ W and an oxygen content in the build chamber of b) 0.04 % and c) 0.2 %.

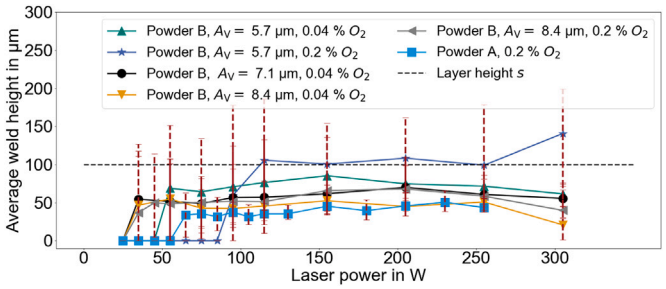

Fig. 4. Average height of the single beads over the laser power for different powders, amplitudes and oxygen contents. A value of zero indicates that no molten material was fused onto the build plate. A scan velocity of $v_s = 700$ mm/s and a layer thickness of $s = 100$ µm were used.

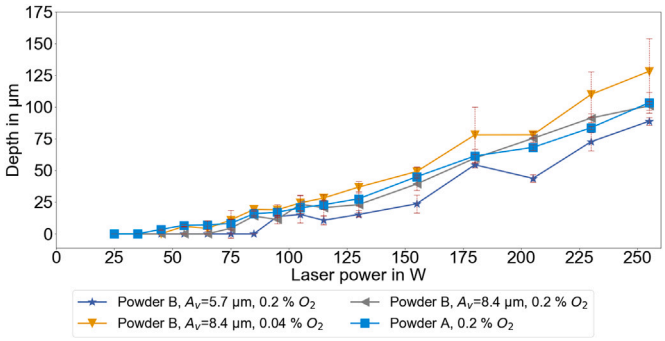

Fig. 6. Melt pool depth vs laser power for different powders, oxygen contents and amplitudes.

higher laser powers, a collision with the sonotrode occurred, and the build job was aborted. For $v_s = 500$ mm/s, the limit is $P = 210$ W. With a higher laser power, contact with the sonotrode occurs. The laser power required to achieve good density values with a scan velocity of $v_s = 700$ mm/s results in a collision with the sonotrode as well. The sonotrode was checked after each build job and the edge was restored if damaged.

The defects of the cube, manufactured with powder B, resulting in the highest density, are shown in Fig. 8(b) [32]. The cube manufactured from powder A with the identical process parameters is shown

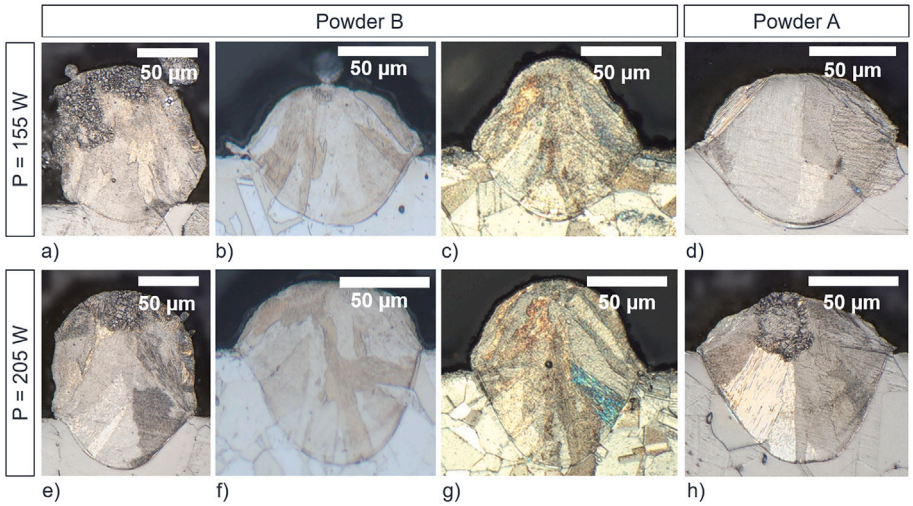

Fig. 5. Images of the cross-section through the single beads. a) and e) amplitude of $A_v = 5.7$ µm and an oxygen content of 0.2 %, b) and f) amplitude of $A_v = 8.4$ µm and an oxygen content of 0.04 %, c) and g) amplitude of $A_v = 8.4$ µm and an oxygen content of 0.2 %, d) and h) rubber lip and an oxygen content of 0.2 %.

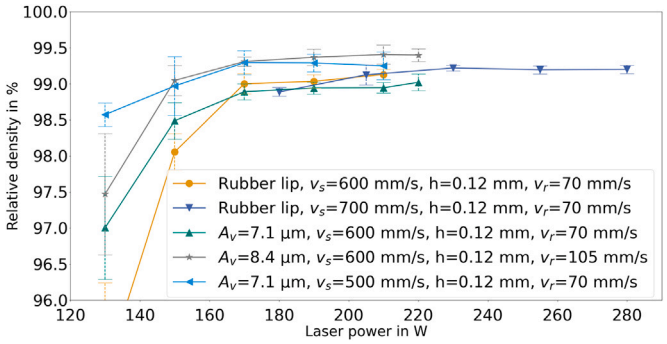

Fig. 7. Relative density for the selection of the best build jobs. The oxygen content in the build chamber is 0.04 % for all build jobs.

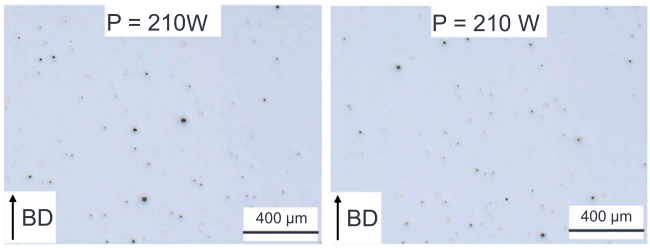

Fig. 8. Defects in the material with $v_s = 600$ mm/s and $P_L = 210$ W for a) powder A and b) powder B [32].

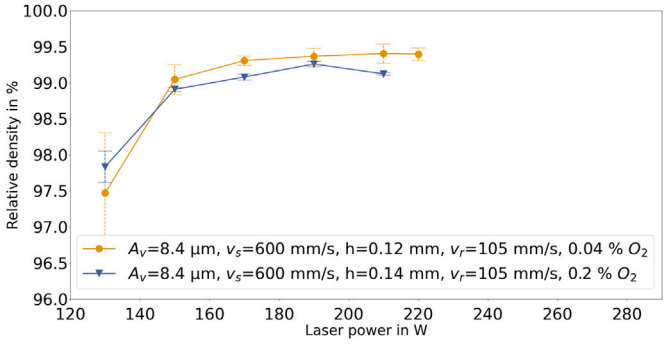

Fig. 9. Relative density for the best build jobs with low and high oxygen content.

for comparison. Both samples show small round pores, confirming the overall density is below 100 %. The sample made from powder A shows slightly larger pores, confirming the lower density compared to powder B.

The sensitivity of powder B to the oxygen content is already shown for the single beads. However, for an amplitude of $A_v = 8.4$ µm the influence could be reduced. Therefore, the process parameters resulting in the highest density for powder B were tested with an initial O_2 content of 0.2 % as well. The start at the higher O_2 content (standard on the machine) reduces the preparation time of a build job by around 20 min, compared to a start at 0.04 %. However, as Fig. 9 shows, the density decreases with a higher oxygen content, when processing powder B.

3.2.2. High speed camera images of the manufacturing process

The images in Fig. 10 show the powder bed right after the laser spot left the image. The laser spot moves from left to right. During the processing of powder A, some individual particles or few particles sticking together are ejected as cold spatter from the powder bed during the process (Fig. 10(a) and b). Some particles are even pushed onto the already scanned tracks, as marked with red squares. However, there is not much difference between the two sets of process parameters.

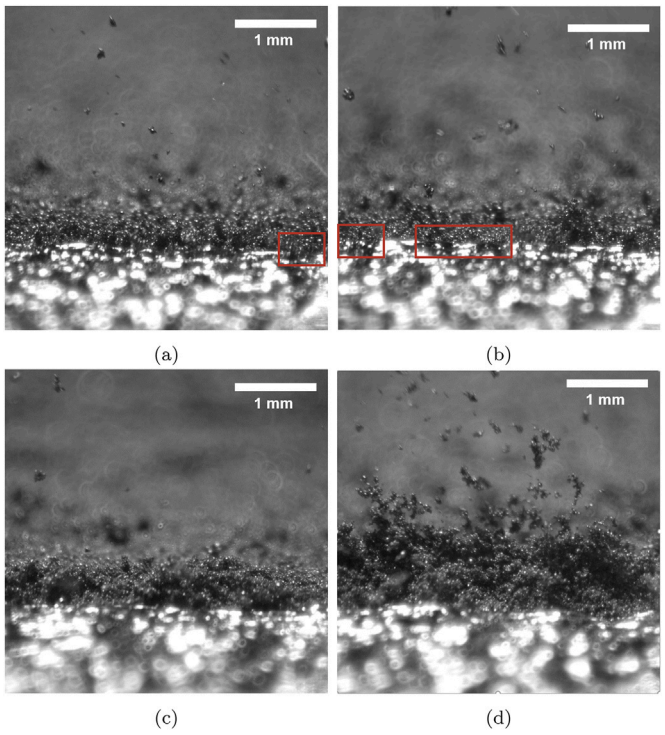

Fig. 10. Image of the current layer right after the laser spot has passed for a) powder A with $v_s = 500$ mm/s and $P = 170$ W, b) powder A with $v_s = 700$ mm/s and $P = 235$ W, c) powder B with $A_v = 8.4$ µm, $v_s = 500$ mm/s and $P = 170$ W, d) powder B with $A_v = 8.4$ µm, $v_s = 700$ mm/s and $P = 235$ W. Powder that was moved onto the already scanned tracks is marked in red.

During the processing of powder B a different phenomena is observed. For $v_s = 500$ mm/s and $P = 170$ W the edge of the powder bed next to the last scanned track is slightly thickened compared to powder A. A few particles are ejected as cold spatter (Fig. 10(c)). However, for $v_s = 700$ mm/s and $P = 235$ W, the movement of the powder bed and the amount of cold spatter is much more intense (Fig. 10(d)). Due to the angle of the camera (Section 2.5), a quantitative measurement of the powder wall height is not possible. A large number of agglomerates are ejected into the air. The smaller once fly several millimeters into the air and are drag to the left by the gas flow. However, the larger agglomerates do not fly far and are not carried away by the gas flow. The large agglomerates in powder B are dragged from the current scan track to the area of the next scan vector by the process induced gas flow. The powder is piled up into a thick powder wall. During the next pass of the laser spot, the powder wall gets pushed further back onto the next scan vector.

4. Discussion

4.1. Stability of single beads

Powder B already has 1.4 times the oxygen content of powder A. This correlates well with the specific surface S_v, which is 1.6 times larger for powder B. Since both powder A and B are from the same batch, the thickness of oxide layer should be comparable. Oxides increase the temperature and the time it takes for molten particles to form a coherent melt pool, due to the cage effect of surface oxide layers [33]. Oxides also decrease the wettability [34]. Chromium as the primary alloying element, but also manganese, have a high affinity to oxygen and form

stable oxides. Even under low oxygen atmosphere, some oxidation cannot be avoided [34]. So overall, the processing of powder B is more challenging due to the higher oxygen content.

In conventional welding, oxides are created through active flux, to increase the penetration of the weld [15]. Therefore, an increased penetration depth could be expected for powder B. However, the opposite effect is observed. The effect of the reduced wettability seems to be dominant, compared to the beneficial effect of the oxides. This explains, why an increased oxygen content has a detrimental effect on the melt pool stability and why powder B is more challenging to process than powder A.

The layer thickness of $s = 100$ µm simulates the PBF-LB\M process with a nominal layer thickness of $s = 50$ µm, due to the increase in real layer thickness within the first few layers [27]. The severe balling and humping for $A_v = 5.7$ µm and 0.2 % initial O_2 content would therefore cause the recoater to collide with solidified material in the next layer. Since the width of the single bead is small at the bottom of the weld track, the average height along the center line of the single bead can be greater than the layer thickness. Even at an O_2 content of 0.04 %, balling and humping still occurs. However, the height of the droplets is reduced. Due to the sensitivity to the oxygen content, there is an indication for an unstable process window, when recoating with an amplitude of $A_v = 5.7$ µm. For an amplitude of $A_v = 8.4$ µm, the sensitivity to oxygen is reduced and a stable single bead forms even for 0.2 % O_2.

The spatter formation correlates with the melt pool stability [14]. However, the presented images from the high speed camera videos don't represent the melting of a single bead. Therefore, a correlation with the single beads is not possible.

To avoid hydrodynamic instabilities like balling or humping and to ensure good binding, remelting of the previous layer is necessary [34].

Balling typically occurs at low energy input, due to little remelting, and the melt pool stabilizes for higher energy inputs [35]. As shown in Fig. 4, this is not the case for powder B recoated with $A_v = 5.7$ µm. Instead, the balling directly changes into a humping condition. Humping is a periodical melt pool fluctuation caused by hydrodynamic instabilities as described above [36]. It occurs at high laser powers, which promote elongated melt pools. At high laser powers, the vapor recoil pressure increases, pushing the melt pool backwards and above the initial surface [36]. This causes the periodical shrinking, known as humping.

Powder B contains much more fine particles, which melt faster and easier than larger ones and start to evaporate even under lower laser powers. Therefore, the vapor recoil pressure is present at much lower laser powers, causing the melt pool to be more prone to humping when processing powder B. This early evaporation might be the reason, why the change to keyhole mode happens at lower laser powers Fig. 6.

At last, the cause for the stabilizing effect of the amplitude needs to be discussed. The measured PLD is above the apparent density at low recoating velocities, indicating that some compacting of the powder takes place during the recoating for powders A and B. However, the PLD is almost identical at low recoating velocities for both amplitudes (Fig. 11).

The PSD of powder B deposited in the powder bed around the cubes was measured after the build job and after the second cycle (Table 6). The d_{10} and d_{50} of powder B increased compared to the virgin state. For the higher amplitude, there is an indication that more fines are removed from the powder. Only one measurement of the PSD was performed.

On the test bench used in [7] to investigate the spreading process, the PSD was not influenced by the amplitude. However, the test bench does not have a circulating gas flow. As shown in [7], agglomerates are not fully dissolved at $A_v = 5.7$ µm, but starting from $A_v = 7.1$ µm a vibro-fluidized state is achieved. With an increase of the amplitude, more of the ultra fine particles are ejected into the air. On the test bench, they fall back down on the build plate and no difference in the PSD is observable. However, in the SLM they get carried away by the circulating gas flow. A detailed investigation of the PSD shows that, for a value of

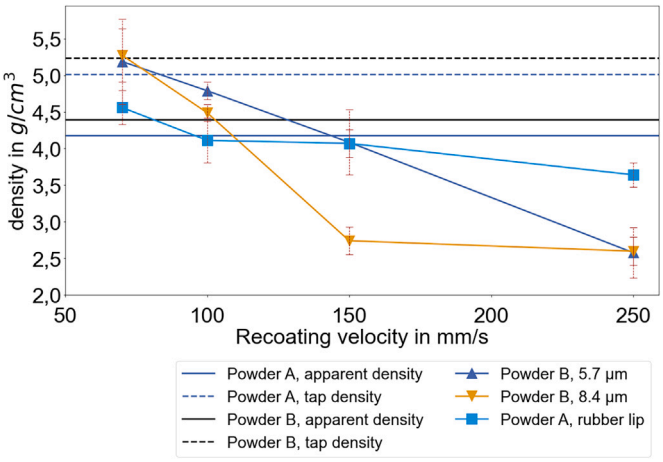

Fig. 11. Powder layer density for different recoater geometries and amplitudes. The apparent density and the tap density are plotted for comparison. The powder layer density for 150 mm/s and 250 mm/s is taken from [7].

Table 6
PSD of powder B in virgin condition and after one and two cycles.

Particle Size	Virgin batch	One cycle $A_v = 7.1$ µm	One cycle $A_v = 8.4$ µm	Two cycles batch
d_{10}	9.96 µm	11.5 µm	12.5 µm	11.8 µm
d_{50}	24.46 µm	24.9 µm	25.8 µm	26.1 µm
d_{90}	49.62 µm	47.6 µm	48.3 µm	49.4 µm

the cumulative size distribution of 0.13 % the particle size $x_{area} = 2.8$ µm for the virgin powder. For the powder which is reused twice, the particle size $x_{area} = 3.2$ µm for the same value of the cumulative size distribution. So the difference comes from ultra fine particles.

Therefore, the amplitude of the sonotrode influences the powder characteristics and subsequently the melting behavior and reaction to the atmospheric oxygen. The removal of the ultra fine particles has two potential benefits for the melt pool stability. First, the evaporation at low laser powers is reduced, preventing the melt pool instabilities. Second, the ultra fine particles have the worst surface-to-volume ratio, containing the most amount of oxides. This stabilizes the melt pool further. The combination of a small amplitude and high oxygen content, creates conditions which are unsuitable for a stable process.

4.2. Process limits of agglomerating powder for volumetric bodies

While a single bead is melted into an undisturbed powder layer, the melting of an area is not uniform, and the weld tracks are influenced by the previous one [18]. The powder moves during the melting due to the process induced gas flow [14,16]. This often leads to denudation of powder around the weld track or ejection of powder particles [10,16]. While the powder movement is well understood for standard powder, agglomerating powder exhibits a completely different behavior.

The powder wall causes an irregular melting behavior and leads to collisions with the recoater during the recoating of the next layer. For the rigid sonotrode, such a collision is particularly critical, since the edge can be damaged and the layer is not recoated evenly. In some cases, even the manufactured cubes show visible damage from the impact (Fig. 12). In case of significant overbuilding causing a collision with the recoater, the build job was aborted to protect the equipment.

This phenomenon of the powder wall occurs at higher laser powers. With increasing scan velocity, the limit for the maximum usable laser power, before a recoating collision occurs, increases as well. A higher scan velocity results in a lower line energy density at the same laser power. As shown by [14], an increase in laser power at the same scan

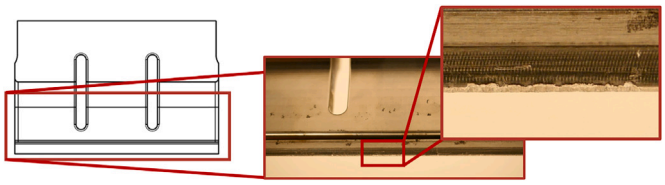

Fig. 12. Image of the recoater after a build job with powder B and $v_s = 700$ mm/s.

velocity increases the amount of spatter and the intensity of the vapor gas flow. Within the resolution of the experiments, $v_s = 600$ mm/s is the maximum scan velocity which can be used for powder B. For higher scan velocities, the required laser power for maximum density leads to the formation of the powder wall.

The process window itself did not change significantly due to the increased amount of fines, only the drop in density for lower laser power was smaller for powder B. This is in accordance to studies with varying, but spreadable, PSDs [37]. At $v_s = 600$ mm/s, for powder B, the density doesn't change significantly starting from $P = 190$ W. At $v_s = 600$ mm/s, for both powder A and B, the best density is achieved with a hatch of h = 0.12 mm and a laser power of $P = 210$ W. Overall, the density of powder B is slightly higher than for powder A. The high densities were achieved in collision free build jobs. The achieved density is comparable [38] or slightly below [1,4] the results of the literature. Even though a successful and collision free build job is possible at higher oxygen contents in the build chamber, the density decreases. This can be explained by two factors. First, this can be due to the reaction of the melt pool with the atmospheric oxygen [9]. As a result, the wettability is reduced, which can induce balling [34,39]. Second, the reaction with the atmospheric oxygen causing the creation of spatter resulting in the formation of pores [17]. Therefore, it is desirable to have an oxygen content as little as possible.

5. Conclusion

In this study, the processing of agglomerating 316 L powder in PBF-LB\M was investigated. The stability of the melt pool was investigated with single beads and the following outcomes can be derived:

- The agglomerating powder (powder B) has a strong tendency for balling or humping and poor wetting of the previous layer. This effect increases, when the oxygen content in the build chamber is higher.
- With an amplitude of $A_v = 8.4$ µm, the melt pool can be stabilized and the height and depth are on a similar level as for the standard powder (powder A).

The stability and process limits for volume bodies were investigated afterward. The following conclusions can be derived:

- A stable processing of the agglomerating powder with a high relative density is possible. The yield of the atomization process can be improved significantly by increasing the amount of fines left in the powder.
- The agglomerating powder can only be processed at reduced scan velocities and laser power. For a higher laser power, the formation of a powder wall, significantly thicker than the powder layer, in the area of the next scan track is observed. This causes a collision with the rigid sonotrode.
- Even though, a collision free processing at 0.2 % initial O_2 content is possible, the density is decreased significantly.

CRediT authorship contribution statement

Kai Drechsel: Writing – original draft, Visualization, Validation, Project administration, Methodology, Investigation, Formal analysis, Data curation, Conceptualization. **Volker Schulze:** Writing – review & editing, Validation, Supervision, Resources, Funding acquisition, Conceptualization. **Frederik Zanger:** Writing – review & editing, Validation, Supervision, Resources, Funding acquisition, Conceptualization.

Declaration of competing interest

The authors declare that they have no known competing financial interests or personal relationships that could have appeared to influence the work reported in this paper.

Acknowledgement

The authors would like to thank Steffen Kramer for the fruitful discussions and encouragement.

Funding

The presented work was funded by the Ministry of Science, Research and the Arts of the Federal State of Baden-Wuerttemberg within the 'InnovationCampus Future Mobility', which is gratefully acknowledged. The project within the 'InnovationCampus Future Mobility' was carried out in cooperation with the PP-Tech GmbH, who funded a proportion of the project.

Data availability

Data will be made available on request.

References

[1] M.A. Spurek, L. Haferkamp, C. Weiss, A.B. Spierings, J.H. Schleifenbaum, K. Wegener, Influence of the particle size distribution of monomodal 316l powder on its flowability and processability in powder bed fusion, Prog. Addit. Manuf. 7 (4) (2022) 533–542, https://doi.org/10.1007/s40964-021-00240-z

[2] F. Chu, E. Li, H. Shen, Z. Chen, Y. Li, H. Liu, S. Min, X. Tian, K. Zhang, Z. Zhou, R. Zou, J. Hou, X. Wu, A. Huang, Influence of powder size on defect generation in laser powder bed fusion of alsi10mg alloy, J. Manuf. Process. 94 (2023) 183–195, https://doi.org/10.1016/j.jmapro.2023.03.046, https://www.sciencedirect.com/science/article/pii/S152661252300261X

[3] P. Fischmann, F. Schrauth, F. Zanger, Influence of particle size distribution on surface roughness in powder bed fusion - a contribution to increase resource efficiency, CIRP Ann. 72 (1) (2023) 145–148, https://doi.org/10.1016/j.cirp.2023.04.018

[4] S. Ziri, A. Hor, C. Mabru, Combined effect of powder properties and process parameters on the density of 316l stainless steel obtained by laser powder bed fusion, Int. J. Adv. Manuf. Technol. 120 (9–10) (2022) 6187–6204, https://doi.org/10.1007/s00170-022-09160-w

[5] M. Xue, X. Chen, X. Ji, X. Xie, Q. Chao, G. Fan, Effect of particle size distribution on the printing quality and tensile properties of ti-6al-4v alloy produced by lpbf process, Metals 13 (3) (2023) https://doi.org/10.3390/met13030604 https://www.mdpi.com/2075-4701/13/3/604

[6] M.A. Balbaa, A. Ghasemi, E. Fereiduni, M.A. Elbestawi, S.D. Jadhav, J.-P. Kruth, Role of powder particle size on laser powder bed fusion processability of alsi10mg alloy, Addit. Manuf. 37 (2021) 101630, https://doi.org/10.1016/j.addma.2020.101630

[7] K. Drechsel, V. Lubkowitz, L. Albrecht, P. Schäfer, M. Schneider, V. Schulze, F. Zanger, Development of an ultrasonically excited recoating process in laser powder bed fusion to process non-spreadable 316l powder, Powder Technol. 432 (2024) 119153, https://doi.org/10.1016/j.powtec.2023.119153

[8] K. Thalberg, D. Lindholm, A. Axelsson, Comparison of different flowability tests for powders for inhalation, Powder Technol. 146 (146 // 3) (2004) 206–213, https://doi.org/10.1016/j.powtec.2004.08.003

[9] M.R. Jandaghi, J. Moverare, Exploring the efficiency of powder reusing as a sustainable approach for powder bed additive manufacturing of 316l stainless steel, Mater. Des. 244 (2024) 113222, https://doi.org/10.1016/j.matdes.2024.113222, https://www.sciencedirect.com/science/article/pii/S0264127524005975

[10] J. Liu, P. Wen, Metal vaporization and its influence during laser powder bed fusion process, Mater. Des. 215 (2022) 110505, https://doi.org/10.1016/j.matdes.2022.110505

[11] Q. Guo, C. Zhao, L.I. Escano, Z. Young, L. Xiong, K. Fezzaa, W. Everhart, B. Brown, T. Sun, L. Chen, Transient dynamics of powder spattering in laser powder bed fusion additive manufacturing process revealed by in-situ high-speed high-energy x-ray imaging, Acta Mater. 151 (2018) 169–180, https://doi.org/10.1016/j.actamat.2018.03.036

[12] R. Rai, J.W. Elmer, T.A. Palmer, T. DebRoy, Heat transfer and fluid flow during keyhole mode laser welding of tantalum, ti–6al–4v, 304l stainless steel and vanadium, J. Phys. D: Appl. Phys. 40 (18) (2007) 5753–5766, https://doi.org/10.1088/0022-3727/40/18/037

[13] Z. Li, G. Yu, X. He, Z. Gan, W.K. Liu, Vapor-induced flow and its impact on powder entrainment in laser powder bed fusion, Mater. Today Commun. 36 (2023) 106669, https://doi.org/10.1016/j.mtcomm.2023.106669

[14] V. Gunenthiram, P. Peyre, M. Schneider, M. Dal, F. Coste, I. Koutiri, R. Fabbro, Experimental analysis of spatter generation and melt-pool behavior during the powder bed laser beam melting process, J. Mater. Process. Technol. 251 (2018) 376–386, https://doi.org/10.1016/j.jmatprotec.2017.08.012
[15] E. Ahmadi, A.R. Ebrahimi, Welding of 316l austenitic stainless steel with activated tungsten inert gas process, J. Mater. Eng. Perform. 24 (2) (2015) 1065–1071, https://doi.org/10.1007/s11665-014-1336-6
[16] Manyalibo J. Matthews, Manyalibo J. Matthews, Manyalibo J. Matthews, Manyalibo J. Matthews, Manyalibo J. Matthews, Manyalibo J. Matthews, Denudation of metal powder layers in laser powder-bed fusion processes, in: Additive Manufacturing Handbook, CRC Press, 2017, pp. 677–692, https://doi.org/10.1201/9781315119106-35
[17] Di Wang, S. Wu, F. Fu, S. Mai, Y. Yang, Y. Liu, C. Song, Mechanisms and characteristics of spatter generation in SLM processing and its effect on the properties, Mater. Des. 117 (2017) 121–130, https://doi.org/10.1016/j.matdes.2016.12.060
[18] J. Wang, R. Zhu, Y. Liu, L. Zhang, Understanding melt pool characteristics in laser powder bed fusion: an overview of single- and multi-track melt pools for process optimization, Adv. Powder Mater. 2 (4) (2023) 100137, https://doi.org/10.1016/j.apmate.2023.100137
[19] DIN EN ISO 15350-08, Stahl und Eisen - bestimmung DER gesamtgehalte an kohlenstoff und schwefel - infrarotabsorptionsverfahren nach verbrennung in einem induktionsofen (standardverfahren) (ISO 15350:2000); Deutsche fassung EN ISO 15350:2010 (2010).
[20] DIN EN 10351:2011-05, Chemische analyse von Eisenwerkstoffen - analyse von unlegierten und niedrig legierten stählen mittels optischer emissionsspektrometrie mit induktiv gekoppeltem plasma - bestimmung von Mn, P, Cu, Ni, CR, Mo, V, Co, Al (gesamt) und Sn [routineverfahren]; Deutsche fassung EN 10351:2011 (2011).
[21] C. des Stahlinstitut VDEh (Ed), Handbuch Für das Eisenhüttenlaboratorium Handbuch Für das Eisenhüttenlaboratorium Band 2 Teil 1, Verl. Stahleisen, Düsseldorf, 2013.
[22] ISO 17053:2005-02 , Stahl und Eisen - Bestimmung des Sauerstofgehaltes - Verfahren mit Infrarotabsorption (2005).
[23] M. Stieß, Mechanische Verfahrenstechnik - Partikeltechnologie 1, Springer Berlin Heidelberg, Berlin, Heidelberg, 2009, https://doi.org/10.1007/978-3-540-32552-9
[24] ASTM B329-24, Test method for apparent density of metal powders and compounds using the scott volumeter (2024).
[25] ASTM B527-4-24, Test method for tap density of metal powders and compounds (2024).
[26] V. Lubkowitz, K. Drechsel, V. Schulze, F. Zanger, Optimization of the layer quality by tic nanoparticles in the ultrasonic excited recoating process with non-spreadable alsi10mg matrix b4c particle-powder composites for powder bed based additive manufacturing, J. Manuf. Process. 126 (2024) 348–357, https://doi.org/10.1016/j.jmapro.2024.07.118
[27] W. Meiners, Direktes selektives laser sintern einkomponentiger metallischer werkstoffe, Dissertation (1999).
[28] W. Wagner, A. Pruß, The IAPWS formulation 1995 for the thermodynamic properties of ordinary water substance for general and scientific use, J. Phys. Chem. Ref. Data 31 (2) (2002) 387–535, https://doi.org/10.1063/1.1461829
[29] P. von Böckh, M. Stripf, Feuchte Luft, In P. von Böckh, M. Stripf (Eds.), Technische Thermodynamik, Springer Berlin Heidelberg, Berlin, Heidelberg, 2015, pp. 413–449, https://doi.org/10.1007/978-3-662-46890-6_10
[30] K. Nagato, T. Ozawa, M. Neuenfeldt, F. Zanger, M. Zhao, V. Schulze, Enhancing the prediction quality of mechanical properties for powder bed fusion with laser beam by dynamic observation of flying particles, Mater. Des. 227 (2023) 111696, https://doi.org/10.1016/j.matdes.2023.111696
[31] C. Kamath, B. El-Dasher, G.F. Gallegos, W.E. King, A. Sisto, Density of additively-manufactured, 316l ss parts using laser powder-bed fusion at powers up to 400 w, Int. J. Adv. Manuf. Technol. 74 (1–4) (2014) 65–78, https://doi.org/10.1007/s00170-014-5954-9
[32] L. Wahl, Ermittlung des Einflusses der pulvergrößenverteilung und Wärmebehandlung auf die Schwingfestigkeit von im PBFLB gefertigten Ultraschallwerkzeugen aus 316l (2023).
[33] X. Yang, F. Gao, F. Tang, X. Hao, Z. Li, Effect of surface oxides on the melting and solidification of 316l stainless steel powder for additive manufacturing, Metall. Mater. Trans. A 52 (10) (2021) 4518–4532, https://doi.org/10.1007/s11661-021-06405-3
[34] S. Das, Physical aspects of process control in selective laser sintering of metals, Adv. Eng. Mater. 5 (10) (2003) 701–711, https://doi.org/10.1002/adem.200310099
[35] D. Gu, Y. Shen, Balling phenomena in direct laser sintering of stainless steel powder: metallurgical mechanisms and control methods, Mater. Des. 30 (8) (2009) 2903–2910, https://doi.org/10.1016/j.matdes.2009.01.013
[36] V. Gunenthiram, P. Peyre, M. Schneider, M. Dal, F. Coste, R. Fabbro, Analysis of laser–melt pool–powder bed interaction during the selective laser melting of a stainless steel, J. Laser Appl. 29 (2) (2017) https://doi.org/10.2351/1.4983259
[37] A.B. Spierings, G. Levy, Comparison of Density of Stainless Steel 316L Parts Produced with Selective Laser Melting Using Different Powder Grades, University of Texas at Austin, 2009.
[38] L. Haferkamp, A. Spierings, M. Rusch, D. Jermann, M.A. Spurek, K. Wegener, Effect of particle size of monomodal 316l powder on powder layer density in powder bed fusion, Prog. Addit. Manuf. 6 (3) (2021) 367–374, https://doi.org/10.1007/s40964-020-00152-4
[39] J.-P. Kruth, L. Froyen, J. Van Vaerenbergh, P. Mercelis, M. Rombouts, B. Lauwers, Selective laser melting of iron-based powder, J. Mater. Process. Technol. 149 (1–3) (2004) 616–622.

Author biography

Kai Drechsel is a graduate of the Karlsruhe Institute of Technology (KIT) and received both his bachelor's and his master's degree in mechanical engineering at KIT. After graduating, he began working at the wbk Institute of Production Science in the research group of Manufacturing and Materials Technology. For his doctoral thesis, he focuses on the experimental and simulative development of an ultrasonically excited recoating process in laser powder bed fusion and the processing of agglomerating 316L powder.

Volker Schulze studied Mechanical Engineering at University Karlsruhe (TH). He received his PhD there in materials technology and worked as Postdoc on mechanical surface and heat treatments. Since 2008 he is one of the directors of wbk Institute of Production Science and also one of the directors of the Institute of Applied Materials at Karlsruhe Institute of Technology. His fields of interests are now mainly manufacturing technologies like cutting and additive manufacturing processes.

Frederik Zanger is an experienced manufacturing engineer in additive manufacturing, machining of metals, simulation of manufacturing processes, and digitalization of process chains. He has established the research group Additive Manufacturing at wbk Institute of Production Science at Karlsruhe Institute of Technology (KIT). As one of the directors of the institute, he holds the chair for digitalization of process development for additive manufacturing since 07/2023. His expertise in additive manufacturing is on powder bed fusion (metals), directed energy deposition (metals), binder jetting (metals) and vat photopolymerization (ceramics) processes.